Mechanical and thermal properties of cellulose nanofiber composites with nanodiamond as nanocarbon filler

Kato, Takashi
Matsumoto, Takuya
Hongo, Chizuru
Nishino, Takashi

(Citation)
Nanocomposites,4(4):127-136

(Issue Date)
2018

(Resource Type)
journal article

(Version)
Version of Record

(URL)
https://hdl.handle.net/20.500.14094/90006108

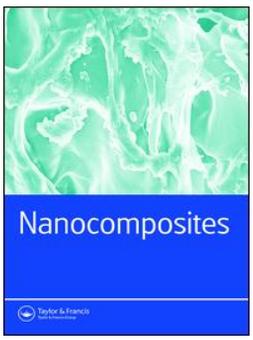

Nanocomposites

ISSN: 2055-0324 (Print) 2055-0332 (Online) Journal homepage: https://www.tandfonline.com/loi/ynan20

Mechanical and thermal properties of cellulose nanofiber composites with nanodiamond as nanocarbon filler

Takashi Kato, Takuya Matsumoto, Chizuru Hongo & Takashi Nishino

To cite this article: Takashi Kato, Takuya Matsumoto, Chizuru Hongo & Takashi Nishino (2018) Mechanical and thermal properties of cellulose nanofiber composites with nanodiamond as nanocarbon filler, Nanocomposites, 4:4, 127-136, DOI: 10.1080/20550324.2018.1550924

To link to this article: https://doi.org/10.1080/20550324.2018.1550924

NANOCOMPOSITES
2018, VOL. 4, NO. 4, 127–136
https://doi.org/10.1080/20550324.2018.1550924

Taylor & Francis
Taylor & Francis Group

RESEARCH ARTICLE

OPEN ACCESS Check for updates

Mechanical and thermal properties of cellulose nanofiber composites with nanodiamond as nanocarbon filler

Takashi Kato, Takuya Matsumoto, Chizuru Hongo and Takashi Nishino

[a]Department of Chemical Science and Engineering, Graduate School of Engineering, Kobe University, Kobe, Japan

ABSTRACT

Cellulose nanofibers are green nanomaterials because of their biodegradability and sustainability, they are also attractive structural materials because of their high mechanical performance. For further expansion of their application and acquisition of their reliability, mechanical reinforcement and functionalization of cellulose nanofiber materials are required. In this work, we focused on the mechanical properties and thermal conductivities of composites of cellulose nanofibers and a nanodiamond (ND). Compared with graphene oxides, which are conventional two-dimensional nanocarbon fillers in aqueous media, natural diamond possesses a much larger modulus. It also has the highest thermal conductivity among all the elemental substances. The ND possesses hydrophilic oxygen functional groups at the surface, following a high dispersion in aqueous media and the rigid diamond structure at the core. In this work, the ND resulted in an increased mechanical reinforcement and enhancement of the thermal conductivity of the cellulose nanofiber, while keeping the high visible light transmittance originating from the latter. In particular, 2,2,6,6-tetramethylpiperidine 1-oxyl-oxidized cellulose nanofibers were reinforced more effectively than quaternary ammonium cellulose nanofibers because of the stronger interaction with the ND and higher dispersibility of the ND. Accordingly, it was proved that the cellulose nanofiber/ND composite was a promising high-strength and high-thermal-conductive material.

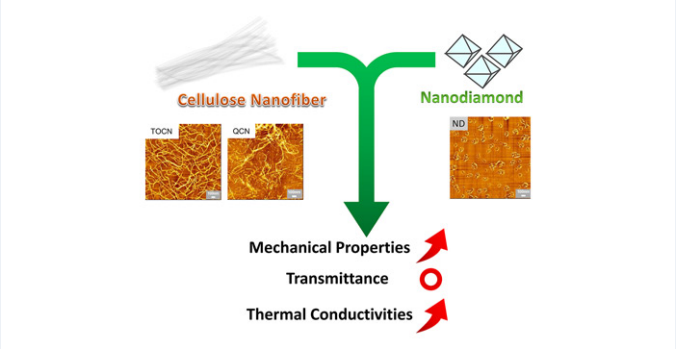

ARTICLE HISTORY
Received 18 September 2018
Accepted 16 November 2018

KEYWORDS
Cellulose nanofiber; nanodiamond; nanocomposite; TEMPO-oxidized CNF; mechanical property; thermal conductivity

Introduction

Cellulose is one of principal components in cell walls [1,2] and has been accepted as an architectural material and hull material since ancient times. Therefore, there is no doubt that cellulose materials are available from eco-friendly and sustainable resources; in addition, they are possess reliable and provide robust mechanical durability [3–11]. Recently, synthetic polymers originating from fossil fuels have been employed as alternatives to metals. From the perspective of environmental conservation and development, bio-based materials including cellulose, a typical biopolymer, are receiving much attention and replacing synthetic polymers. In addition, for achieving an increased material performance, various bio-based polymers have been composited with diverse nanofillers [3,5,11–13].

Nanocarbon materials, such as fullerene [14,15], carbon nanotube [16–19], graphene [20–24], graphene oxide (GO) [25–30] and nanodiamond (ND) [31–37], have attracted attention in the various fields of photovoltaic devices, spin electronics and structural materials. ND is prepared by a detonation method, can be dispersed in aqueous media because

*CONTACT Takashi Nishino tnishino@kobe-u.ac.jp Department of Chemical Science and Engineering, Graduate School of Engineering, Kobe University, Rokko, Nada, Kobe 657-8501, Japan.

Supplemental data for this article can be accessed at https://doi.org/10.1080/20550324.2018.1550924.

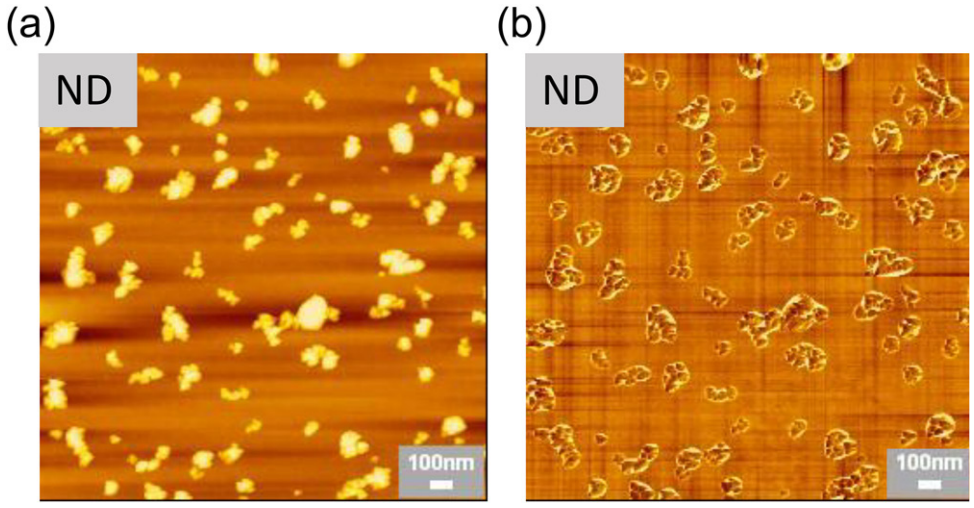

Figure 1. Atomic force microscope (AFM) (a) topological and (b) phase images of ND.

of the presence of hydrophilic oxygen functional groups at their surface, and have a spherical shape with approximately 10 nm diameter, as shown in Figure 1 [38]. Recently, ND has become purchasable as a commercial product. Natural diamond possesses a supremely large modulus (1 TPa) and the highest thermal conductivity (2200 W/(m K)) among all the elemental substances. Therefore, ND is accepted as a mechanical- and thermal-reinforcement filler in composites owing to their large modulus and thermal stability [28,36,37,39,40].

For this decade, cellulose nanofiber is a prominent research topic as a 'green' and 'nano' material owing to its robust mechanical properties [10,11]. Cellulose nanofiber is used not only as a reinforcement filler but also as a high-performance matrix [12,13,41–43]. Various preparation methods of cellulose nanofibers have been reported; for example, mechanical grounding method, microfluidics method, chemically modified method and enzyme fibrillation [11,44–52]. Particularly, the major chemical nanofibrillation methods are the 2,2,6,6-tetramethylpiperidine 1-oxyl (TEMPO)-mediated oxidation treatment reported by Isogai et al. [6,9,44,51] and quaternary ammonium treatment using glycidyltrimethylammonium chloride (GMAC) reported by Ho et al. [46,53,54] The functional groups and surface properties of cellulose nanofibers are controlled by these chemical nanofibrillation methods. For achieving effective reinforcements in nanocomposites, their high dispersion in aqueous media and strong interaction with nanofillers are significant. Actually, nanocomposites composed of cellulose nanofibers and nanocarbon fillers such as carbon nanotubes and graphene have been reported. The low dispersity of these nanocarbon fillers in aqueous media is problematic for the improvement of mechanical defects in their composites [55–57].

Herein, we focused on the cellulose nanofiber composites with chemically nanofiberized celluloses as matrixes and ND as fillers for mechanical reinforcement and thermal conductive enhancement, and therefore, investigated their mechanical properties and thermal conductivities [35,40]. The effects of GO fillers on the mechanical and thermal properties of the cellulose nanofiber composites were also evaluated and compared with the results of the ND loading.

Materials and methods

Materials

Bast fibers of kenaf (*Hibiscus cannabinus*, Indonesia, 2011) were provided by Toyota Boshoku Co. (Aichi, Japan), which are accepted as 'green composite materials' in the motor vehicle industry such as the world-leading company TOYOTA Co. Ltd. ND aqueous dispersion of 2.75 wt%, which had a diameter of approximately 10 nm, was provided by Bando Co. Ltd. (Japan). For comparison, 1.0 wt% Nano GRAX (Mitsubishi Gas Co. Ltd.) in an aqueous dispersion was also employed as graphene oxide; its diameter was approximately 3 μm and thickness was from 0.5 nm to 1 nm. Toluene, sodium chlorite, sodium hypochlorite, acetic acid, potassium hydroxide, sodium bromide, sodium hydroxide, hydrochloric acid, oxalic acid, benzene and silver nitrate were purchased from Nacalai Tesque Co. Ltd. Ethanol, carbon tetrachloride, carbon tetrachloride were purchased from Wako Co. Ltd. TEMPO was purchased from Hydrus Chemical Inc. GMAC and 1.0 M bis(ethylenediamine)copper(II) hydroxide in H_2O were purchased from Sigma-Aldrich Co. LLC. All the chemicals were used without further purification.

Purification of cellulose from kenaf

Based on the reported literature [58], refined pulp was purified from rough kenaf bast fibers by

removing grease with toluene/ethanol eluents, lignin with Wise methods and hemicellulose using alkaline treatment. Kenaf bast fibers, 20 g, were degreased via Soxhlet extraction using a 1:2 (v/v) mixture of ethanol/toluene for 20 h at 78 °C (78 °C: azeotropic temperature). The Kenaf-bast fibers were then washed thrice with ethanol and dried in vacuo at 50 °C for 12 h. A residual fraction of the degreased biomass was suspended in 1 L of distilled water, and the following treatment was applied. To remove the lignin from a sample, sodium chlorite, 6.7 g, was directly added to the biomass suspension described above with gentle mixing, and acetic acid, 1.2 mL, was subsequently added. The biomass suspension mixture was then incubated at 80 °C for 1 h. The addition of sodium chlorite, 6.7 g, and acetic acid, 1.2 mL, was repeated five times in 1-h intervals. Finally, the mixture was filtered using filter paper No. 1 (Advantech Toyo Kaisha, Ltd., Tokyo, Japan), and the solid fraction was rinsed five times with distilled water. The rinsed sample was maintained in a semi-wet state at 4 °C until use. To eliminate the hemicellulose from the biomass, the degreased biomass was allowed to dry (or semi-wet biomass after Wise treatment), then it was soaked with 4 wt% potassium hydrate solution, 0.5 L, at 80 °C for 2 h. The reaction mixture was filtered with filter paper No. 1, and the filtrate sample was rinsed thrice with distilled water. This operation was repeated twice. Finally, the mixture was filtered using filter paper No. 1, and the solid fraction was rinsed five times with distilled water. The rinsed sample was maintained in a semi-wet state at 4 °C until use.

Preparation of TEMPO-mediated cellulose nanofiber (TOCN)

The purified kenaf fibers were oxidized by TEMPO by reported methods [59]. Sodium bromide (NaBr), 1.0 g, and TEMPO, 0.16 g, were added to 1 L of distilled water and dissolved. The purified kenaf fibers, 10 g, were added to this solution, followed by addition of 25 mL of 1 M sodium hypochlorite (NaClO) solution. The pH of the solution was maintained at 10 by titrating 0.5 M sodium hydroxide (NaOH) for 10 h with an automatic titration apparatus (AUT-501, DKK-TOA Co., Tokyo, Japan). After the titration, the treated cellulose was filtered and washed with excess distilled water to remove the excess reactants and impurities. TEMPO-oxidized cellulose hydrogels were obtained after the washing steps, and they were dispersed in 800 mL of acetate buffer (pH 4.8). Sodium chlorite (9.1 g) was added to oxidize the residual aldehyde groups to carboxyl groups. After washing the resulted oxidized cellulose fibers with excess distilled water, the concentration was adjusted to 0.4 wt% for fibrillation treatment. Briefly, 0.4 wt% oxidized cellulose aqueous solutions were fibrillated using a high-speed mixer (MX1200XT, Xtreme Hi-Power Blender, Waring, TX, USA) at 22,000 rpm for 10 min and the TEMPO-oxidized cellulose nanofiber (TOCN) was obtained.

Preparation of quaternary ammonium cellulose nanofiber (QCN)

The purified kenaf fibers were reacted with GMAC, and quaternary ammonium cellulose nanofibers (QCN) were prepared as per the reported method [46]. Prefibrillation of the purified kenaf fiber aqueous dispersion (dried weight: 20 g) was performed at 22,000 rpm for 30 min with a high-speed mixer (MX1200XT, Xtreme Hi-Power Blender, Waring, TX, USA). The pulverized kenaf fibers were centrifuged with 9000×*g* at 12 °C for 5 min using a centrifugal separator (M201-IVD, Sakuma Co. Ltd.), and the water was removed by decantation. The solid fraction was mercerized in 10 wt% sodium hydroxide aqueous solution at 70 °C for 1 h. After centrifugation of the mercerized samples, the solid fraction and 13.3 g sodium hydroxide were added into 140 mL deionized water and stirred. GMAC, 55 mL, was added to the solution and stirred at 70 °C for 4 h. After stirring, 37 mL GMAC was added again and stirred at 70 °C for 4 h. After the reaction, the pH of the solution was controlled at approximately 2 with hydrochloric acid and the dispersion was filtered. The samples were dispersed in deionized water, the pH was again controlled at 3, and then the samples were stirred for 24 h. The filtration and dispersion were repeated 10 times. The dispersion was performed with grinding treatments using a grinder instrument (MKCA6-2, Masuko Sangyo Co. Ltd.) at 1500 rpm with three passes. QCN was obtained as aqueous dispersion.

Preparation of CNF, CNF/ND and CNF/GO composites

We added 2.75 wt% ND or 1.0 wt% GO aqueous dispersion into 260 mL of 0.25 wt% TOCN or QCN dispersion. The dispersions were defoamed and filtered. The obtained samples were dried at 40 °C for 12 h. TOCN/ND composites (TND 1 wt%, TND 2.5wt%, TND 5 wt%, TND 10 wt%, TND 33 wt% and TND 50 wt%) and QCN/ND composites (QND 1 wt%, QND 2.5wt%, QND 5 wt%, QND 10 wt%, QND 33 wt% and QND 50 wt%) were obtained. However, only the QND 50 wt% composite was not formed as a composite because of its fragility (see Figures S6, S7 in the Supporting Information). In the case of GO, TOCN/GO composites (TGO

0.5wt%, TGO 1 wt%, TGO 2.5wt%, TGO 5 wt% and TGO 10 wt%)and QCN/GO composites (QGO 0.5wt%, QGO 1 wt%, QGO 2.5wt%, QGO 5 wt% and QGO 10 wt%) were also prepared (see Figure S8, S9 in the Supporting Information).

Characterizations

A Fourier transform infrared (FT-IR) spectrophotometer (Perkin Elmer, Ltd., Spectrum GX FT-IR System I-KS) was used for the investigation of the functional groups of each sample. The dried (under vacuum oven at 40 °C for 48 h) samples were dispersed in KBr pellets. The prepared samples were measured in a range between 400 and 4000 cm^{-1} with 2 cm^{-1} resolutions for 10 times accumulation.

An atomic force microscope (AFM) (Nano Navi E-sweep, Hitachi, Tokyo, Japan) was used for the observation of the TOCN, QCN and ND. The TOCN and QCN on mica substrates were observed with a dynamic mode AFM in topological images.

Conductometric titration was performed, and the conversion ratios of the carboxyl groups on the surface of the TOCN were evaluated. The frozen TOCN hydrogels were dried under vacuum for 1 day to obtain cryogels. The TOCN cryogel (0.05 g) was then dispersed in deionized water (130 mL) with addition of 10 mL of 0.01 M sodium chloride (NaCl) solution under stirring. The pH of the aqueous dispersion was controlled at 2.8 using sodium hydroxide solution and hydrochloric acid solution. Then, the dispersion was titrated with 0.07 M sodium hydroxide solution at 0.1 mL/min rate using an automatic titrator (AUT-501, TOA-DKK Co. Ltd.) and electrical conductometer (CM-60V, TOA-DKK Co. Ltd.). The density of the carboxyl group in the prepared TOCNs was calculated from the amount of sodium hydroxide consumed during the coordination of the sodium ions to the carbonyl groups by the following equation.

$$\text{Carboxyl group density (mmol/g)} = \frac{\text{NaOH (L)} \times \text{NaOH concentration (M)} \times \text{NaOH factor}}{\text{Sample mass (g)}}$$

During the measurement of the amount of quaternary ammonium in the QCN, conductometric titration was also performed. QCN cryogel (0.05 g) was dispersed in 110 mL deionized water. The dispersion was titrated with 0.005 M silver nitrate solution at 0.2 mL/min rate using an automatic titrator (AUT-501, TOA-DKK Co. Ltd.) and electrical conductometer (CM-60V, TOA-DKK Co. Ltd.). The density of quaternary ammonium in the prepared QCN was calculated from the amount of silver nitrate consumed during the titration by following equation.

$$\text{Quaternary ammonium group density (mmol/g)} = \frac{\text{AgNO}_3\text{ (L)} \times \text{AgNO}_3\text{ concentration (M)} \times \text{AgNO}_3\text{ factor}}{\text{Sample mass (g)}}$$

The measurements of the molecular weights of the TOCN and QCN were performed. CNF cryogels, 125 mg, were dispersed in 10 mL deionized water and stirred for several days. Bis(ethylenediamine) copper(II) hydroxide solution (5 mL of 0.5 M) was added and stirred for 5 min. In addition, the TOCN or QCN was dissolved by adding 10 mL of 1.0 M bis(ethylenediamine)copper(II) hydroxide solution and stirring for 20 min. The viscosities of the obtained solutions were measured, and the intrinsic viscosity number $[\eta]$ and viscosity-average molecular weights M_v were calculated [60].

X-ray diffraction profiles were obtained using RINT-Ultima +2200 (Rigaku Co. Ltd.) with a symmetrical reflection geometry. CuKα beam ($\lambda = 1.5418$ Å) was generated at 40 kV and 20 mA. The scanning speed was 2°/min, and the sampling step was 0.02°. The crystallinity X_c was calculated by Segal's method [61]. The crystallite size originated from 200 reflections was estimated using the Scherrer equation [62,63].

Thermogravimetry analyses (TGA) were performed with a Thermo plus EVO 2 series (TG8121, Rigaku Co. Ltd.) in a N_2 atmosphere from 150 to 550 °C. The temperature for 5 wt% loss was defined as the thermal degradation temperature T_{5d}.

UV–vis absorbance measurements were performed with a Jasco V-750 UV/Vis spectrometer. The scan speed was 400 nm/min, and the range of the wavelength was from 200 to 900 nm.

Density was measured by the floatation method with benzene ($d = 0.88$ g/cm^3)/tetrachloromethane ($d = 1.60$ g/cm^3) system at 30 °C.

The mechanical properties of the TOCN and QCN and the TND, QND, TGO and QGO composite sheets were measured with a tensile tester (Autograph, AGS-1kND, Shimadzu Co. Ltd.). The initial length was 20 mm, and the tensile speed was 1.0 mm/min. The tensile tests were performed using more than five individual specimens. The cross sectional areas of the samples were evaluated from the densities, lengths and weights of the samples.

For the calculation of the specific heat capacities of the TOCN and QCN and the TND, QND, TGO and QGO composites, RIGAKU DSC8230 was used. Al_2O_3, 10 mg, was used as a standard sample. From the following equation, the specific heat capacity was calculated.

$$C_{ps} = \frac{C_{pr} \times m_r}{Y_r} \times \frac{Y_s}{m_s} \quad (1)$$

where C_{ps} and C_{pr} are the specific heat capacities of the samples and Al_2O_3 standard, and m_s and m_r

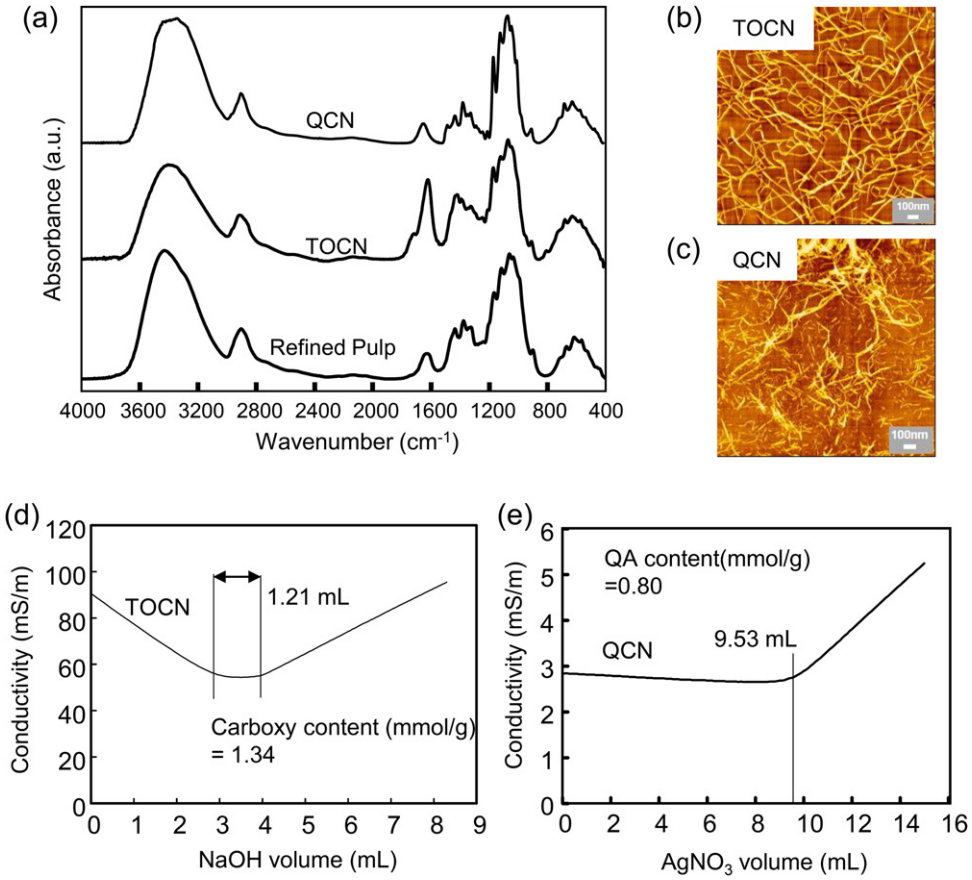

Figure 2. (a) FT-IR spectra of the TOCN and QCN, AFM topological images of (b) TOCN and (c) QCN, and electric conductometric curves of the (d) TOCN and (e) QCN.

are their weights. Y_s denotes the difference between the DSC curves of the samples and empty Al pan, and Y_r is the difference between the DSC curves of the standard and empty Al pan.

For the measurement of the thermal diffusivity by the periodic heating and infrared radiation thermometer method, we used Thermowave Analyzer TA3 (Bethel Co. Ltd.). Thermal diffusivities α for the in-plane and thickness directions were measured. Before the measurements, the samples were blackened by carbon spray for periodic heating with a laser. Thermal conductivities λ were calculated from the following equation.

$$\lambda = \alpha \cdot \rho \cdot C_{ps} \quad (2)$$

where $\cdot\rho$ represents the densities of the samples.

Results and discussion

We prepared the TOCN and QCN from the bast fibers of kenaf by TEMPO-mediated oxidation and quaternary ammonium treatment, respectively. The obtained TOCN and QCN were characterized by FT-IR, AFM and conductometric titration, as shown in Figure 2. In the FT-IR spectrum of the TOCN, an increase in the carboxyl absorption bands at 1615 cm^{-1} were observed, which indicated that the hydroxyl groups at the 6-position of cellulose were translated to carboxyl groups [59]. The carboxyl groups were included with a concentration of 1.34 mmol/g. The concentration of the carboxyl groups in the refined pulps was 0.24 mmol/g. These results imply that the TEMPO-oxidation of the hydroxyl groups at the 6-position has fairly progressed. The AFM observation revealed that the TOCN possesses a diameter of 2.8 nm, and high aspect ratio, whereas the diameter of the raw kenaf bast fiber was approximately 10 µm. The FT-IR absorption bands of the QCN originating from the quaternary ammonium groups were observed at 1480 cm^{-1} [53]. From the conductometric titration measurements, it is estimated that the quaternary ammonium groups had a concentration of 0.80 mmol/g, whereas their concentration in the refined pulps was approximately 0 mmol/g. These indicate that the quaternary ammonium groups are certainly included. The AMF topological images of the QCN confirm the completion of the nanofibrillation and reveal that the QCN diameters were 6.4 nm. The aspect ratio of the QCN was smaller than that of the TOCN. In addition, after nanofibrillation, both the TOCN and QCN remain kept well dispersed in aqueous media for more than several days.

The molecular weights of the TOCN and QCN in bis(ethylenediamine)copper(II) hydroxide solution

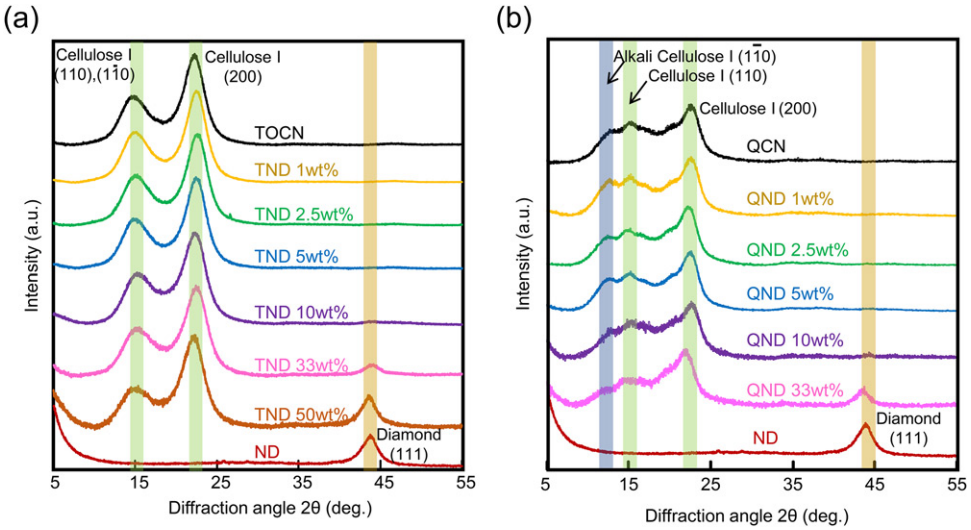

Figure 3. X-ray diffraction profiles of the (a) TND composites and (b) QND composites.

were evaluated using intrinsic viscosity number measurements. The results are presented in Table S1 in the Supporting Information. Before nanofibrillation, the molecular weight of the refined pulp was more than 350k, whereas those of TOCN and QCN were 128k and 130k, respectively, which were lower relative to that of the refined pulp. This was because TEMPO-oxidation and mercerization under alkali condition led to cleavage of the β-glycoside bonds in cellulose, i.e. β-elimination, and consequently decreased the length of the cellulose main chains. These nanofibrillated celluloses with these molecular weights possessed sufficient mechanical durability toward their mechanical and functional measurements.

For the investigation of the crystallites in the composites, X-ray diffraction measurements were performed for all the prepared composites. In the TND composites, the diffraction peaks (see Figure 3) originating from the (1 1 0)/(1 − 1 0) and (2 0 0) planes of cellulose I were observed at $2\theta = 15.2°$, 22.4°, respectively [11]. In the case of the QTD composites, the diffraction peak at 12.5° originating from the (1 − 1 0) plane of alkali cellulose I overlapped with that of cellulose I. In addition, both the TND and QTD composites, including those with more than 10 wt% ND, showed a diffraction peak originating from the (1 1 1) plane of diamond at $2\theta = 44°$. These results imply that the ND was incorporated in the TOCN and QCN without any change and deterioration of the crystalline structure of each component.

Figure S2 in the Supporting Information shows the TGA thermograms of the prepared composites and Table S2 in the Supporting Information lists their decomposition temperature and ND content ratio estimated from the residual weights at 500 °C. The temperature where the samples lost 5 wt% of their weight, T_{d5}, of the TND composites increased with the ND content. Thus, the NDs having a high thermal stability interacted with the TOCN matrixes and reinforced the TND composites thermally. In contrast, the T_{d5} of the QND composites remained constant, even with the ND loading. The ND contents, estimated from the residual weights at 500 °C, were mostly in agreement with the ratios of the CNFs and ND in the recipe. In addition, we observed the cross section of the TND and QND using FE-SEM and evaluated the dispersity of the ND in the TOCN and QCN matrixes, as shown in Figures S3 and S4 in the Supporting Information. In those SEM images, agglomeration of the ND was not observed. These results indicated the high dispersion of the ND in these cellulose matrixes.

Figure 4 shows the UV–vis transmittance spectra of the TND and QND composites containing 0, 1, 2.5, 5 and 10 wt% of the ND. The TOCN and TND composites, even including that with 10 wt% ND, have a higher transmittance relative to the QCN and QND composites, respectively. The reason for the lower transmittance of the QND is the high visible light scattering of the QCN itself. For the evaluation of the loading effect of the ND on the transmittance, the transmittance results of the TGO and QGO composites were also investigated. The UV–vis transmittance spectra of the TGO and QGO composites are presented in Figure S5 in the Supporting Information. GO has been widely accepted as a reinforcement carbon nanofiller in aqueous dispersion systems [64,65]. The transmittances of even the TGO and QGO composites including that with only 0.5 wt% GO, clearly decreased. There is no doubt regarding the advantage of the transmittance of the TND and QND composites over the GO-based composites. Their visible appearance also supported these results, as shown in Figures S6–S9 in the Supporting Information.

For the evaluation of the reinforcement effects of the ND fillers in the TOND and QND composites,

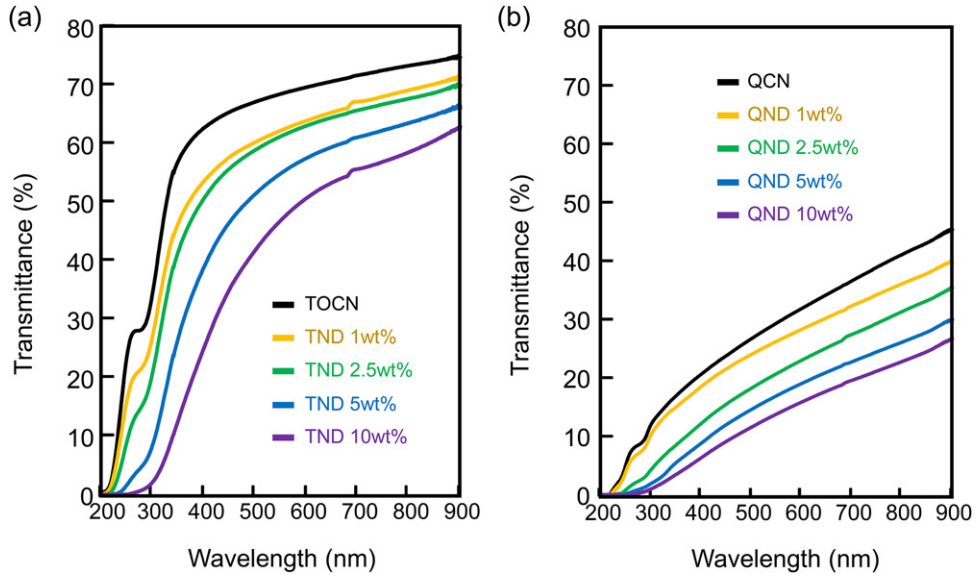

Figure 4. UV–vis transmittance spectra of the (a) TND composites and (b) QND composites. All the transmittances were normalized as films with 50-μm thickness.

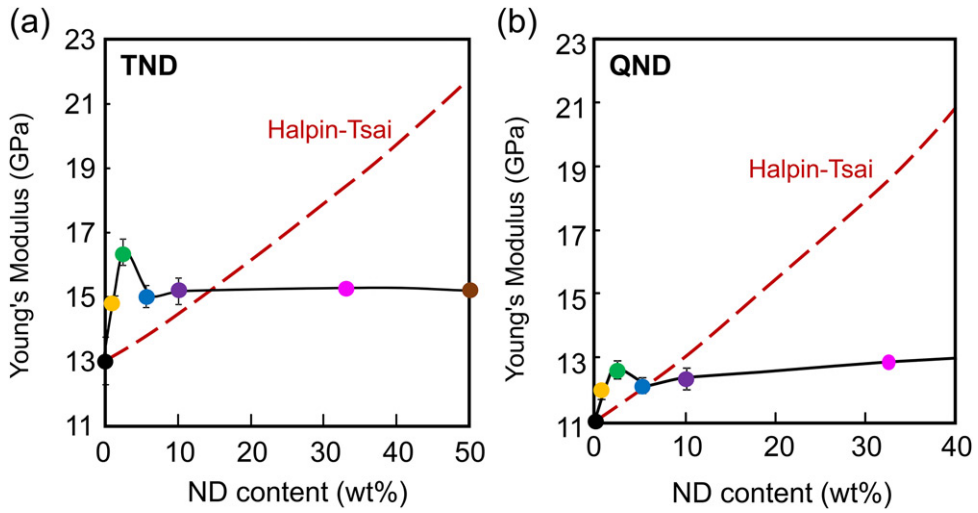

Figure 5. Young's modulus of the (a) TND composites and (b) QND composites and (broken line) theoretical Young's modulus based on the Halpin–Tsai models.

their tensile tests were performed. Figure S10 and Table S3 in the Supporting Information present these results. All the composites had a larger Young's modulus than that of the TOCN and QCN sheets. The Young's modulus of the TND and QND composites first increased and then decreased with the ND loading. The reason was that excess ND in TND and QND composites agglomerated and acted as defects. For insight into the reinforcement effects of the ND, the TGO and QGO composites were compared. Their Young's moduli are presented in Figure S11 in the Supporting Information. The Halpin–Tsai models are considered on the basis of the moduli of the fillers being well-dispersed in the matrixes and not on the interaction between the fillers and matrixes [66]. As shown in Figure 5, the Young's moduli of the TND and QND composites with less than 10 wt% of ND were larger than the theoretically estimated values based on the Halpin–Tsai models, whereas those of both the TGO and QGO composites were inferior to those of the theoretical models regardless of the ND content. These trends can be a result of the larger reinforcement effect of the ND on the TOCN and QCN. In addition, it is suggested that the ND could interact more strongly with TOCN and disperse more in TOCN than in QCN. The tensile strengths and elongation at the peak of the TND composites, including less than 10 wt% ND, increased, whereas for more than 10 wt% ND, they decrease. The reason is the agglomeration of the excess ND in the TND composites introduced mechanical defects. In contrast, the tensile strengths and elongation at peak of the QND composites were decreased by adding the ND filler. The difference between the TND and QND composites may be attributed to the dispersibility and interaction of the ND fillers with the cellulose nanofiber matrixes.

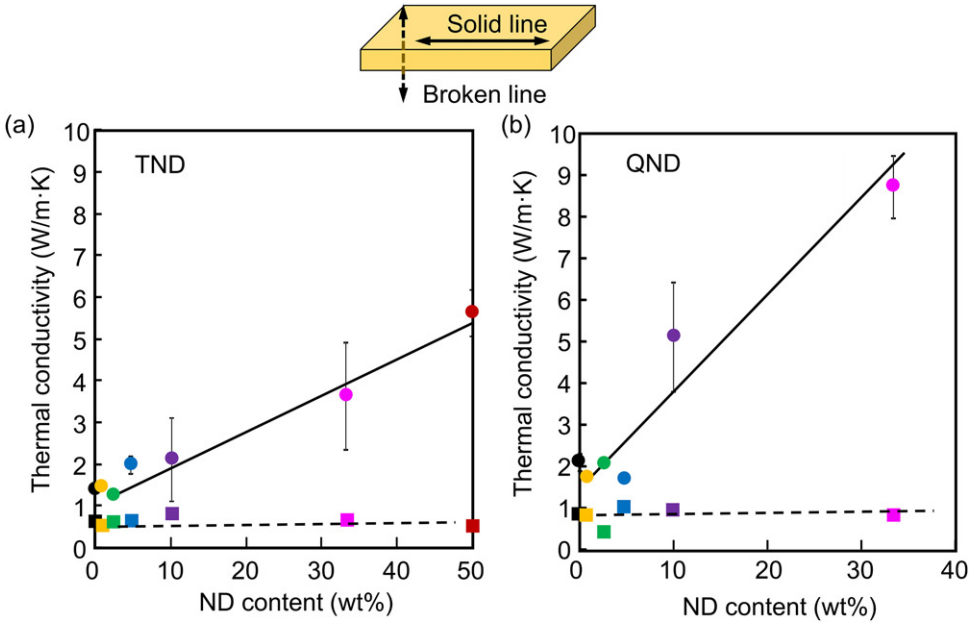

Figure 6. Thermal conductivities of the (a) TND composites and (b) QND composites. Circles show the thermal conductivities in the in-plane direction and squares show those in the thickness direction.

The thermal conductivities of the TND and QND in the (solid line) in-plane and (broken line) thickness directions are shown in Figure 6. In the TND and QND composites, the thermal conductivities in the thickness direction remain constant, whereas those in the in-plane direction increase with increasing amount of the ND. CNFs with high aspect ratios, such as TOCN and QCN, are known to orient parallel to the surface in the sheets and possess layered structure [64], with the ND laid between their layers in the parallel direction. This could be a reason for the increase in their thermal conductivities in in-plane direction. The thermal conductivities of the TGO and QGO were remained constant or increased slightly, as shown in Figure S12 in the Supporting Information. These results suggested that ND had more advantages as thermal conductive fillers that GO.

Conclusions

In this study, we prepared TND and QND composites and evaluated their optical, mechanical and thermal properties. The ND reinforced the cellulose nanofiber matrixes mechanically and enhanced their thermal conductivity while maintaining their high visible light transmittance. The effects of the ND on the TND composites were more significant than those on the QND composites because of the stronger interaction and higher dispersity of the ND in the TOCN. In addition, the ND fillers exhibited more advantages in terms of the reinforcement and enhancement of the mechanical and thermal properties relative to graphene oxide, which was selected as an alternative carbon filler in aqueous media. These results indicated that the TND and QND composites could be promising high-thermal conducting materials with a high-mechanical strength.

Disclosure statement

No potential conflict of interest was reported by the authors.

Funding

This study was supported by the Core Research for Evolutional Science and Technology (CREST, JPMJCR13B2), and Japan Science and Technology Agency (JST).

References

1. Cosgrove DJ. Growth of the plant cell wall. Nat Rev Mol Cell Biol. 2005;6:850.
2. Somerville C, Bauer S, Brininstool G, et al. Toward a systems approach to understanding plant cell walls. Science. 2004;306:2206–2211.
3. Nishino T, Peijs T. Handbook of green materials. Vol. 5. New York (NY): World Scientific; 2013. p. 201–216.
4. Nishino T. In: C. Baillie, editor. Woodhead publishing series in composites science and engineering. Cambridge (UK): Woodhead Publishing; 2004. p.49–80.
5. Nishino T. In: C. Baillie and R. Jayasinghe, editors. Woodhead publishing series in composites science and engineering. Cambridge (UK): Woodhead Publishing; 2017. p.19–38.
6. Isogai A. Development of completely dispersed cellulose nanofibers. Proc Jpn Acad Ser B: Phys Biol Sci. 2018;94:161–179.
7. Sakurada I, Nukushina Y, Ito T. Experimental determination of the elastic modulus of crystalline regions in oriented polymers. J Polym Sci. 1962;57:651–660.

8. Nishino T, Takano K, Nakamae K. Elastic modulus of the crystalline regions of cellulose polymorphs. J Polym Sci B: Polym Phys. 1995;33:1647–1651.
9. Saito T, Kuramae R, Wohlert J, et al. An ultrastrong nanofibrillar biomaterial: the strength of single cellulose nanofibrils revealed via sonication-induced fragmentation. Biomacromolecules. 2013;14:248–253.
10. El-Hosseiny F, Page DH. The mechanical properties of single wood pulp fibres: theories of strength. Fibre Sci Technol. 1975;8:21–31.
11. Eichhorn SJ, Dufresne A, Aranguren M, et al. Review: current international research into cellulose nanofibres and nanocomposites. J Mater Sci. 2009; 45:1–33.
12. Siró I, Plackett D. Microfibrillated cellulose and new nanocomposite materials: a review. Cellulose. 2010;17:459–494.
13. Mohanty AK, Misra M, Hinrichsen G. Biofibres, biodegradable polymers and biocomposites: an overview. Macromol Mater Eng. 2000;276–277:1–24.
14. Ajayan PM. Nanotubes from carbon. Chem Rev. 1999;99:1787–1800.
15. Thompson BC, Fréchet JMJ. Polymer–fullerene composite solar cells. Angew Chem Int Ed. 2008;47: 58–77.
16. Iijima S. Helical microtubules of graphitic carbon. Nature. 1991;354:56.
17. Thess A, Lee R, Nikolaev P, et al. Crystalline ropes of metallic carbon nanotubes. Science. 1996;273: 483–487.
18. Wang G, Zhang L, Zhang J. A review of electrode materials for electrochemical supercapacitors. Chem Soc Rev. 2012;41:797–828.
19. Coleman JN, Khan U, Blau WJ, et al. Small but strong: A review of the mechanical properties of carbon nanotube–polymer composites. Carbon. 2006;44:1624–1652.
20. Novoselov KS, Fal'Ko VI, Colombo L, et al. A roadmap for graphene. Nature. 2012;490:192.
21. Geim AK. Graphene: status and prospects. Science. 2009;324:1530–1534.
22. Castro Neto AH, Guinea F, Peres NMR, et al. The electronic properties of graphene. Rev Mod Phys. 2009;81:109–162.
23. Schwierz F. Graphene transistors. Nat Nanotechnol. 2010;5:487.
24. Rao CNR, Sood AK, Subrahmanyam KS, et al. Graphene: the new two-dimensional nanomaterial. Angew Chem Int Ed Engl. 2009;48:7752–7777.
25. Dreyer DR, Park S, Bielawski CW, et al. The chemistry of graphene oxide. Chem Soc Rev. 2010;39: 228–240.
26. Zhu Y, Murali S, Cai W, et al. Graphene and graphene oxide: synthesis, properties, and applications. Adv Mater. 2010;22:3906–3924.
27. Morimune-Moriya S, Ariyoshi M, Goto T, et al. Ultradrawing of poly(vinyl alcohol)/GRAPHENE oxide nanocomposite fibers toward high mechanical performances. Compos Sci Technol. 2017;152:159–164.
28. Morimune S, Kotera M, Nishino T, et al. Uniaxial drawing of poly(vinyl alcohol)/graphene oxide nanocomposites. Carbon. 2014;70:38–45.
29. Morimune S, Nishino T, Goto T. Poly(vinyl alcohol)/graphene oxide nanocomposites prepared by a simple eco-process. Polym J. 2012;44:1056–1063.
30. Morimune S, Nishino T, Goto T. Ecological approach to graphene oxide reinforced poly (methyl methacrylate) nanocomposites. ACS Appl Mater Interfaces. 2012;4:3596–3601.
31. Ho D, Wang C-HK, Chow EK-H. Nanodiamonds: the intersection of nanotechnology, drug development, and personalized medicine. Sci Adv. 2015;1: e1500439.
32. Aharonovich I, Greentree AD, Prawer S. Diamond photonics. Nat Photon. 2011;5:397.
33. Schrand AM, Hens SAC, Shenderova OA. Nanodiamond particles: properties and perspectives for bioapplications. Crit Rev Solid State Mater Sci. 2009;34:18–74.
34. Mochalin VN, Shenderova O, Ho D, et al. The properties and applications of nanodiamonds. Nat Nanotechnol. 2011;7:11.
35. Morimune-Moriya S, Salajkova M, Zhou Q, et al. Reinforcement effects from nanodiamond in cellulose nanofibril films. Biomacromolecules. 2018;19: 2423–2431.
36. Morimune S, Kotera M, Nishino T, et al. Poly(vinyl alcohol) nanocomposites with nanodiamond. Macromolecules. 2011;44:4415–4421.
37. Morimune S, Nishino T. High performance polymer composites with nanocarbon materials. Fiber. 2013;69:70–76.
38. Ōsawa E. Recent progress and perspectives in single-digit nanodiamond. Diam Relat Mater. 2007;16: 2018–2022.
39. Kidalov SV, Shakhov FM, Vul' AY. Thermal conductivity of nanocomposites based on diamonds and nanodiamonds. Diam Relat Mater. 2007;16: 2063–2066.
40. Song N, Cui S, Hou X, et al. Significant enhancement of thermal conductivity in nanofibrillated cellulose films with low mass fraction of nanodiamond. ACS Appl Mater Interfaces. 2017;9: 40766–40773.
41. Jonoobi M, Harun J, Mathew AP, et al. Mechanical properties of cellulose nanofiber (CNF) reinforced polylactic acid (PLA) prepared by twin screw extrusion. Compos Sci Technol. 2010;70:1742–1747.
42. Iwatake A, Nogi M, Yano H. Cellulose nanofiber-reinforced polylactic acid. Compos Sci Technol. 2008;68:2103–2106.
43. Bhatnagar A, Sain M. Processing of cellulose nanofiber-reinforced composites. J Reinf Plast Compos. 2005;24:1259–1268.
44. Isogai A, Saito T, Fukuzumi H. TEMPO-oxidized cellulose nanofibers. Nanoscale. 2011;3:71–85.
45. Davoudpour Y, Hossain S, Khalil HPSA, et al. Optimization of high pressure homogenization parameters for the isolation of cellulosic nanofibers using response surface methodology. Ind Crops Prod. 2015;74:381–387.
46. Ho TTT, Zimmermann T, Hauert R, et al. Preparation and characterization of cationic nanofibrillated cellulose from etherification and high-shear disintegration processes. Cellulose. 2011;18:1391–1406.
47. Okita Y, Saito T, Isogai A. Entire surface oxidation of various cellulose microfibrils by TEMPO-mediated oxidation. Biomacromolecules. 2010;11: 1696–1700.
48. Henrissat B, Claeyssens M, Tomme P, et al. Cellulase families revealed by hydrophobic cluster analysis. Gene. 1989;81:83–95.

49. Janardhnan S, Sain MM. Isolation of cellulose microfibrils—an enzymatic approach. Bioresources. 1:176–188.
50. Enebro J, Momcilovic D, Siika-Aho M, et al. Investigation of endoglucanase selectivity on carboxymethyl cellulose by mass spectrometric techniques. Cellulose. 2009;16:271–280.
51. Isogai A. Wood nanocelluloses: fundamentals and applications as new bio-based nanomaterials. J Wood Sci. 2013;59:449–459.
52. Abdul Khalil HPS, Davoudpour Y, Islam MN, et al. Production and modification of nanofibrillated cellulose using various mechanical processes: a review. Carbohydr Polym. 2014;99:649–665.
53. Pei A, Butchosa N, Berglund LA, et al. Surface quaternized cellulose nanofibrils with high water absorbency and adsorption capacity for anionic dyes. Soft Matter. 2013;9:2047–2055.
54. Hasani M, Cranston ED, Westman G, et al. Cationic surface functionalization of cellulose nanocrystals. Soft Matter. 2008;4:2238–2244.
55. Yamakawa A, Suzuki S, Oku T, et al. Nanostructure and physical properties of cellulose nanofiber-carbon nanotube composite films. Carbohydr Polym. 2017;171:129–135.
56. Li Y, Zhu H, Wang Y, et al. Cellulose-nanofiber-enabled 3D printing of a carbon-nanotube microfiber network. Small Methods. 2017;1:1700222.
57. Zhang T, Zhang X, Chen Y, et al. Green fabrication of regenerated cellulose/graphene films with simultaneous improvement of strength and toughness by tailoring the nanofiber diameter. ACS Sustain Chem Eng. 2018;6:1271–1278.
58. Nobuta K, Teramura H, Ito H, et al. Characterization of cellulose nanofiber sheets from different refining processes. Cellulose. 2016;23:403–414.
59. Fujisawa S, Okita Y, Fukuzumi H, et al. Preparation and characterization of TEMPO-oxidized cellulose nanofibril films with free carboxyl groups. Carbohydr Polym. 2011;84:579–583.
60. Klemm W, Philipp D, Heinze B, et al. Comprehensive cellulose chemistry. New York (NY): Wiley; 2004.
61. Segal L, Creely JJ, Martin AE, et al. An empirical method for estimating the degree of crystallinity of native cellulose using the X-ray diffractometer. Text Res J. 1959;29:786–794.
62. Kakudo M, Kasai N. X-ray diffraction by polymers. Tokyo: Kodansha; 1972.
63. Patterson AL. The Scherrer formula for X-ray particle size determination. Phys Rev. 1939;56:978–982.
64. Yang W, Zhao Z, Wu K, et al. Ultrathin flexible reduced graphene oxide/cellulose nanofiber composite films with strongly anisotropic thermal conductivity and efficient electromagnetic interference shielding. J Mater Chem C. 2017;5:3748–3756.
65. Gao K, Shao Z, Wu X, et al. Cellulose nanofibers/reduced graphene oxide flexible transparent conductive paper. Carbohydr Polym. 2013;97:243–251.
66. Shanmuganathan K, Capadona JR, Rowan SJ, et al. Stimuli-responsive mechanically adaptive polymer nanocomposites. ACS Appl Mater Interfaces. 2010;2:165–174.